SINTEF
PROCEEDINGS
2

Proceedings of the 12th International Conference on Computational Fluid Dynamics in the Oil & Gas, Metallurgical and Process Industries

Progress in Applied CFD – CFD2017

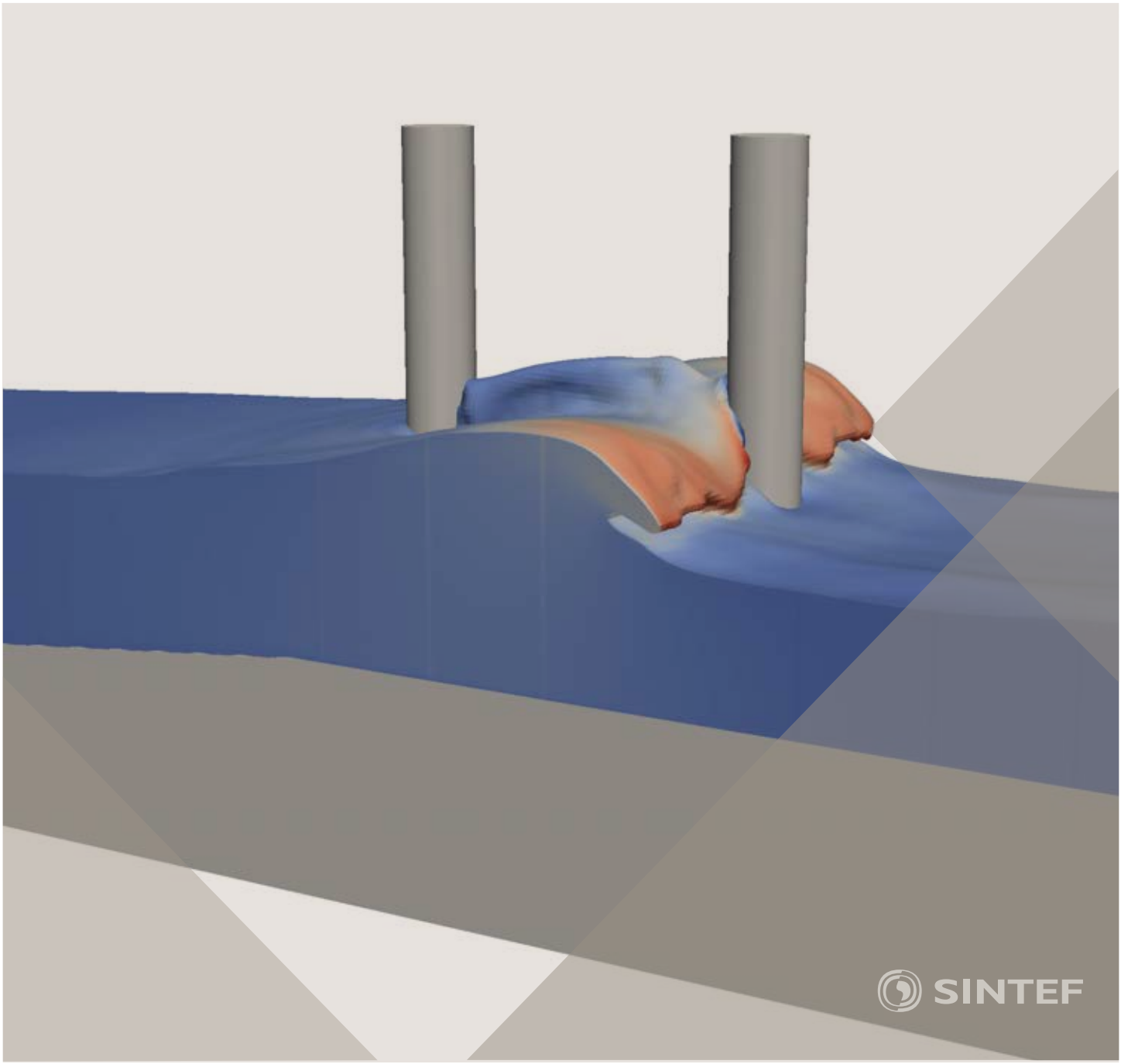

SINTEF Proceedings

Editors:
Jan Erik Olsen and Stein Tore Johansen

Progress in Applied CFD – CFD2017

Proceedings of the 12th International Conference on Computational Fluid Dynamics in the Oil & Gas, Metallurgical and Process Industries

SINTEF Academic Press

SINTEF Proceedings no 2
Editors: Jan Erik Olsen and Stein Tore Johansen
Progress in Applied CFD – CFD2017
Selected papers from 10th International Conference on Computational Fluid Dynamics in the Oil & Gas, Metallurgical and Process Industries

Key words:
CFD, Flow, Modelling

Cover, illustration: Arun Kamath

ISSN 2387-4295 (online)
ISBN 978-82-536-1544-8 (pdf)

SINTEF Academic Press
Address: Forskningsveien 3 B
PO Box 124 Blindern
N-0314 OSLO
Tel: +47 73 59 30 00
Fax: +47 22 96 55 08

www.sintef.no/byggforsk
www.sintefbok.no

SINTEF Proceedings
SINTEF Proceedings is a serial publication for peer-reviewed conference proceedings on a variety of scientific topics.
The processes of peer-reviewing of papers published in SINTEF Proceedings are administered by the conference organizers and proceedings editors. Detailed procedures will vary according to custom and practice in each scientific community.

PREFACE

This book contains all manuscripts approved by the reviewers and the organizing committee of the 12th International Conference on Computational Fluid Dynamics in the Oil & Gas, Metallurgical and Process Industries. The conference was hosted by SINTEF in Trondheim in May/June 2017 and is also known as CFD2017 for short. The conference series was initiated by CSIRO and Phil Schwarz in 1997. So far the conference has been alternating between CSIRO in Melbourne and SINTEF in Trondheim. The conferences focuses on the application of CFD in the oil and gas industries, metal production, mineral processing, power generation, chemicals and other process industries. In addition pragmatic modelling concepts and bio-mechanical applications have become an important part of the conference. The papers in this book demonstrate the current progress in applied CFD.

The conference papers undergo a review process involving two experts. Only papers accepted by the reviewers are included in the proceedings. 108 contributions were presented at the conference together with six keynote presentations. A majority of these contributions are presented by their manuscript in this collection (a few were granted to present without an accompanying manuscript).

The organizing committee would like to thank everyone who has helped with review of manuscripts, all those who helped to promote the conference and all authors who have submitted scientific contributions. We are also grateful for the support from the conference sponsors: ANSYS, SFI Metal Production and NanoSim.

Stein Tore Johansen & Jan Erik Olsen

Organizing committee:

Conference chairman: Prof. Stein Tore Johansen
Conference coordinator: Dr. Jan Erik Olsen
Dr. Bernhard Müller
Dr.Sigrid Karstad Dahl
Dr.Shahriar Amini
Dr.Ernst Meese
Dr.Josip Zoric
Dr.Jannike Solsvik
Dr.Peter Witt

Scientific committee:

Stein Tore Johansen, SINTEF/NTNU
Bernhard Müller, NTNU
Phil Schwarz, CSIRO
Akio Tomiyama, Kobe University
Hans Kuipers, Eindhoven University of Technology
Jinghai Li, Chinese Academy of Science
Markus Braun, Ansys
Simon Lo, CD-adapco
Patrick Segers, Universiteit Gent
Jiyuan Tu, RMIT
Jos Derksen, University of Aberdeen
Dmitry Eskin, Schlumberger-Doll Research
Pär Jönsson, KTH
Stefan Pirker, Johannes Kepler University
Josip Zoric, SINTEF

CONTENTS

12th International Conference on CFD in Oil & Gas, Metallurgical and Process Industries
SINTEF, Trondheim, NORWAY
May 30th - June 1st, 2017

A DNS STUDY OF DROPLET SPREADING AND PENETRATION ON A POROUS MEDIUM

S DAS[1]*, **E MILACIC**[1], **H.V. PATEL**[1], **N.G. DEEN**[2], **J.A.M. KUIPERS**[1]

[1]Multiphase Reactors Group, Dept. of Chemical Engineering and Chemistry, Eindhoven University of Technology, P.O. Box 513, 5600 MB Eindhoven, The Netherlands

[2]Multiphase and Reactive Flows Group, Department of Mechanical Engineering, Eindhoven University of Technology, P.O. Box 513, 5600 MB Eindhoven,The Netherlands

* E-mail: s.das@tue.nl

ABSTRACT

We have investigated the dynamics of droplet spreading and liquid penetration at the surface of a porous medium at zero-gravity condition. A coupled IBM-VOF finite volume code has been used to perform pore-scale level fully resolved numerical simulations. The geometrical details of the solid porous matrix are resolved by a sharp interface immersed boundary method (IBM) on a Cartesian grid, whereas the motion of the gas-liquid interface is tracked by a mass conservative volume of fluid (VOF) method. At small scales, the contact line dynamics mainly govern the spreading and capillary penetration. In the present case, the motion of the gas-liquid interface at the immersed boundary is modeled by imposing the contact angle as a boundary condition at the three-phase contact line. All the simulations are performed using a model porous structure that is approximated by a 3D cubic scaffold with cylindrical struts. The porosity (ε) of the porous structure is varied from $\varepsilon = 0$ (flat plate) to $\varepsilon = 0.65$ and the equilibrium contact angle Θ is varied from $\Theta = 30^{\circ}$ (hydrophilic) to $\Theta = 135^{\circ}$ (hydrophobic). The effect of porosity and contact angle on the transient evolution of penetration and spreading have been presented and compared with classical models.

Keywords: Three phase flow, immersed boundary method (IBM), volume of fluid (VOF), contact line dynamics, capilary penetration
.

NOMENCLATURE

Notations

p	Pressure, $[Pa]$
t	Time, $[s]$
D	Droplet diameter, $[m]$
F	Fluid phase fraction, $[-]$
H	Droplet height, $[m]$
La	Laplace number, $[-]$
S	Spreading diameter, $[m]$
V	Penetration volume, $[m^3]$

Greek Symbols

ρ	Mass density, $[kg/m^3]$
μ	Dynamic viscosity, $[Pa \cdot s]$
σ	Surface tension, $[N/m]$
Θ	(Static) contact angle, $[degree]$
ε	Porosity, $[-]$
τ	Non-dimentional time, $[-]$
$\bar{\bar{\tau}}$	Stress tensor, $[N/m^2]$

Vectors

$\mathbf{u}$	Velocity, $[m/s]$
$\mathbf{F}_\sigma$	Surface tension force, $[N]$
$\mathbf{g}$	Gravitational acceleration, $[m/s^2]$

Sub/superscripts

V_0	Total droplet volume, $[m^3]$

INTRODUCTION

When a droplet of liquid is placed on the surface of a solid substrate, the liquid interface will evolve until it reaches an equilibrium condition. Depending on liquid-gas, solid-liquid and liquid-gas surface tensions, the liquid droplet attains a finite angle with the solid surface and this can be described by Young's equation. While Young's equation assumes that the surface is smooth, the equilibrium contact angle Θ depends on, (i) surface roughness or surface topography (μm scale) and (ii) material properties that involve intermolecular forces acting at the very thin meniscus of liquid film at the gas-liquid-solid contact line acts at *nm* scale. On engineering scales, for very slow flow for a given gas-liquid-solid system it can be assumed that Θ is fixed (i.e. a static contact angle) throughout the evolution of droplet from initial to equilibrium condition. In absence of gravity, at the equilibrium condition, the droplet will always remain a spherical cap and the intermediate motion of the gas-liquid interface is governed by the relative contribution of the surface tension, liquid inertia and viscous forces. A series of experimental and numerical studies (Yang and Xu, 2017; Frank and Perre, 2012; Legendre and Maglio, 2013) are available in the literature which deals with the transient evolution of the droplet shape in presence of a flat solid surface. The present work deals with understanding the wetting, spreading and capillary imbibition of a liquid droplet in contact with a *porous surface* or *porous structure.* This phenomenon is important for many engineering applications and scientific research, such as ink-jet printing, enhanced oil recovery (EOR), several micro-fluidics devices, biological systems, surface coating of porous material etc. The typical length scale of the porous medium is in the order of $\sim 10^{-3} m$ and it can be assumed that the evolving droplet maintains a constant equilibrium contact angle (Θ) with each parts of the porous structure.

Numerical prediction of the dynamics of a droplet in contact with a porous structure demands a state-of-the-art direct numerical model/ technique for coupling the contact line

motion at the solid surface and capillary penetration. As a result very few fully resolved pore-scale level numerical simulations area available attacking this complex flow behavior. Frank et al. (Frank and Perre, 2012; Frank *et al.*, 2015) performed a direct numerical simulation for droplet spreading on a porous medium using a lattice Boltzmann method (LBM) under zero gravity conditions. In their study, a porous structure made of longitudinal cavities is considered, that only allows the capillary penetration unidirectionaly. The motion of the fluid in the transverse direction, inside the porous structure is restricted, which is not a true representation of a realistic porous medium. They have chosen a system of low Laplace number (ratio of surface tension to momentum transport) for smooth motion of the liquid. Meng *et al.* (2014) performed a similar pore-scale level study using smoothed particle hydrodynamics (SPH) in a model porous medium with and without gravity condition. Hyväluoma *et al.* (2006) performed pore-resolved LBM simulations for droplet penetration in paper board. 3D micro-tomographic images of paper board were used in their numerical study.

In the present work, the porous structure is approximated by a 3D cubic scaffold with cylindrical struts, where motion of the liquid in both the longitudinal and transverse directions are studied. The geometrical details of the solid porous matrix are resolved by a sharp interface immersed boundary method (IBM) (Deen *et al.*, 2012; Das *et al.*, 2016) on a Cartesian grid, whereas the motion of the gas-liquid interface is tracked by a mass conservative volume of fluid (VOF) method (Van Sint Annaland *et al.*, 2005). The motion of the gas-liquid interface at the immersed boundary is modeled by imposing the contact angle as a boundary condition at the three-phase contact line (Patel *et al.*, 2017).

GOVERNING EQUATIONS AND SOLUTION METHODOLOGY

In the present single-field/ single-equation formulation for two-fluid flows, the mass and momentum conservation equations for both the fluids are given as follows:

$$\nabla \cdot \mathbf{u} = 0 \tag{1}$$

$$\rho \frac{\partial \mathbf{u}}{\partial t} + \rho \nabla \cdot (\mathbf{u}\mathbf{u}) = -\nabla p + \nabla \cdot \bar{\bar{\tau}} + \rho \mathbf{g} + \mathbf{F}_\sigma \tag{2}$$

where $\bar{\bar{\tau}} = \mu[\nabla \mathbf{u} + (\nabla \mathbf{u})^T]$ is the fluid stress tensor; ρ and μ are local averaged density and viscosity. The volumetric source term $\mathbf{F}_\sigma$ appearing in the momentum equation is due to surface tension (σ) between the two fluids and acts only in the vicinity of the interface (Brackbill *et al.*, 1992). The dynamics of the interface is captured by a Volume of Fluid (VOF) method (Van Sint Annaland *et al.*, 2005) where the two different fluids are identified by a color function F. It indicates the fractional amount of fluid present at a certain computational cell. The motion of the interface is evoluted by advecting the color function (F) with the local fluid velocity as,

$$\frac{\partial F}{\partial t} + \mathbf{u} \cdot \nabla F = 0 \tag{3}$$

In Eq. 2, the local density (ρ) is calculated by linear averaging of the densities of the fluid 1 and fluid 2. However, the local viscosity (μ) is calculated by harmonic averaging of the kinematic viscosities of the individual fluid phases. A geometrical advection scheme is used to solve Eq. 3 which allows to achieve a very high degree of mass conservation.

In the Cartesian domain, the no-slip condition at the solid non-conforming boundary is imposed by an implicit (direct) second-order accurate Immersed Boundary Method (IBM) (Deen *et al.*, 2012; Das *et al.*, 2016). In the presence of fluid-fluid interfaces with immersed solids, contact line dynamics plays a major role in wetting phenomena. It is incorporated by applying the apparent contact angle (Θ) as a boundary condition for interface at the contact lines (Patel *et al.*, 2017). The effect of the contact angle is taken into account by modifying the fluid-fluid interface normals at the solid boundaries. The detailed implementation and thorough validation of the present IBM-VOF coupling strategy has been reported in Patel *et al.* (2017).

RESULTS AND DISCUSSIONS

Droplet spreading on a flat plate

As a base case, we start with analyzing the droplet spreading on a flat surface. When a spherical droplet is placed gently on a flat surface, at the very first instance the air layer between the droplet and the surface is drained; and a small liquid bridge is formed between the drop and the surface. To maintain the wettability condition, an initial perturbation travels upward in the form of a capillary wave. If the fluid has a large inertia for a very small Θ, the larger size of the capillary waves may raise up to the drop surface and 'pinch-off' may occur. The Laplace number ($La = \frac{\rho\sigma 0.5D}{\mu^2}$), compares the inertia and surface tension to viscosity effect, and can be used as a dimensionless quantity to predict droplet pinch-off. At a very high La, the capillary wave and eventual pinch-off of the droplet may create satellite droplets.

If we study the transient development of wetted area, characterised by the equivalent spreading diameter $S(t)$), for a completely wetting case ($\Theta \approx 0$), the droplet spreading phenomena can be divided into an early stage inertia dominant wetting, following a power-law $S(t) \sim t^n$ with $n = \frac{1}{2}$ and a second stage consisting of a viscous regime, where $n = \frac{1}{10}$, according to Tanner's law (Tanner, 1979). Varying the relative contributions between the inertia, viscous force, surface tension and gravity different evolutions have been reported in the literature: $n = 1/8, 1/7, 1/5, 1/4$. To check the accuracy of our numerical model, at first we have studied droplet spreading on a flat surface using the same settings of experimental work by Winkels *et al.* (2012). The flat surface is represented by an immersed surface at the $[1\,1\,1]$ plane, which does not conform the Cartesian grid. Across the diameter of the droplet 40 grid cells are used. In Fig. 1 the transient evolution of spreading diameter is shown. Similar to the experiments, a water droplet in air has been considered which corresponds to $La = 36 \times 10^3$. As a results the initial spreading is purely governed by the inertial force and we expect $S(t) \sim t^{0.5}$ as temporal evolution. The spreading diameter (S) is non-dimensionalized by the initial diameter of the droplet (D) and time (t) is normalized by the inertial scale, i.e. $\tau = t/(\rho(D/2)^3/\sigma)^{0.5})$. In sub-fig (a) to (d) the simulations snapshots are presented: (a) initial spherical droplet, (b) capillary wave propagating in the upward direction, (c) pinch-off at the upper portion of the droplet and (d) at the end of inertial spreading leaving a spherical cap shape of the droplet. After inertial spreading the bubble interface oscillates a few times before it finally reaches the equilibrium condition. Fig. 1 shows a very good match with experiments and indeed we observe a $\sim t^{0.5}$

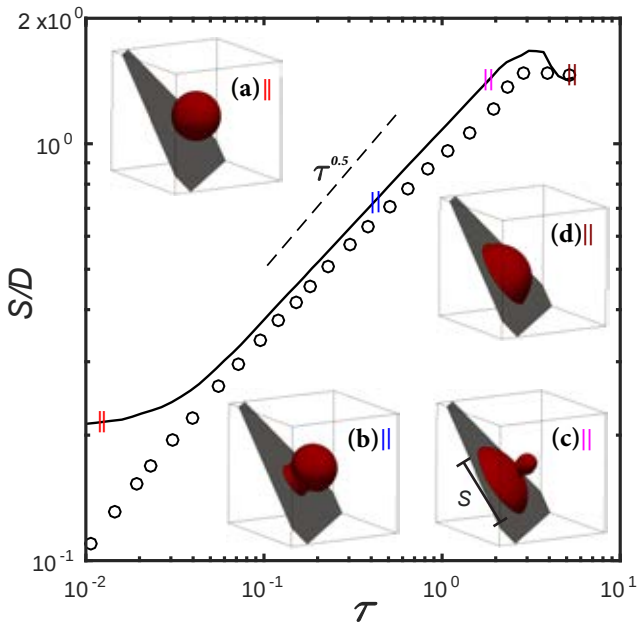

Figure 1: Transient evolution of spreading diameter (S/D) with non-dimentionalised time (τ) for droplet spreading on a flat surface with $\Theta = 65°$. In a Cartesian grid the flat surface is represented as an immersed surface. The line indicates the simulation results and the markers are for the experimental results. The simulation snapshots at four different time intervals are also shown.

evolution of spreading diameter. Please note, unlike the experimental results, in our simulation the initial spreading radius is not zero due to finite grid resolution. In reality, at the very beginning, there exists a point contact (zero surface area) between the droplet and the solid surface. However, due to the finite grid resolution in our numerical simulation there will always be some overlap between the droplet and surface to initiate the spreading. At very high grid resolution $S(0) \to 0$, nevertheless with the current grid resolution we are able to capture the $S(t) \sim t^n$ trend very accurately.

Droplet spreading and capillary penetration on a porous block

The computational setup of the main system studied in this work is shown in Fig. 2, where a liquid droplet is put in contact with a porous block. Each ligament and each pore size of the porous structure is resolved by at least 12 grid cells. The simulations are performed in a single quarter of the domain using a symmetry boundary condition. The total number of computational cells are reported as $\sim 9 \times 10^6$. The time-step size ($\sim 10^{-6}\, s$) has been restricted by both the CFL and capillary wave constraint (Patel *et al.*, 2017). The diameter (D) of the droplet is 4 mm and the fluid properties are: $\mu = 0.034\, Pa-s$, $\rho = 809\, kg/m^3$ and $\sigma = 0.032\, N/m$. The surrounding medium is air. It corresponds to an air-squalane oil system with $La = 45$. The porous block is made of equidistant cylindrical ligaments and the size of the representative elementary volume (REV) is 0.67 mm. Due to the capillarity and the wetting condition, the droplet spreads as well as penetrates inside the porous slab. Porous structures of three different porosities, $\varepsilon = 0.35$, 0.5 and 0.65 have been considered. The equilibrium contact angle (Θ) between the air-oil interface with the solid ligaments is varied from 30° to 135°. As $La = 45$, spreading is dominated by inertia. However, the magnitude of the capillary wave is not very

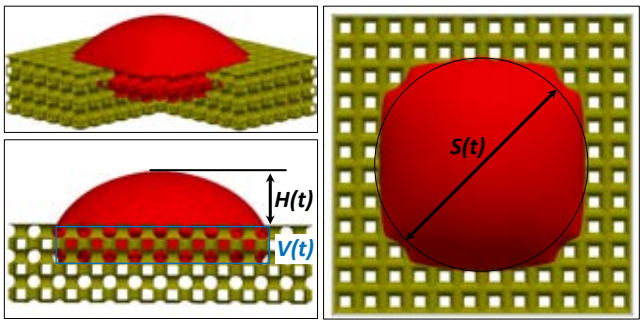

Figure 2: Droplet spreading and capillary penetration on a porous block: physical description of the problem. $H(t)$ represents the transient evolution of the height of the droplet, $S(t)$ represents the equivalent spreading radius and the penetration volume is represented by $V(t)$.

vigorous to pinch-off the droplet from its top surface. At each time-step we capture the droplet height (H), the equivalent spreading diameter (S) at the porous surface and the volume of the penetrated liquid (V).

The transient development of droplet shape, spreading and capillary imbibition are shown in Fig. 3 for a typical case ($\varepsilon = 0.5$ and $\Theta = 30°$). Please notice that the simulation snapshots are not taken at equal intervals. From the initial position ($\tau = 0$) to $\tau = 1.03$, the upper portion of the droplet does not move, liquid slightly penetrates inside the porous structure and finally forms a cylindrical shape. In reality, when the droplet touches the solid, to satisfy the wetting condition, a perturbation is generated generates at the contact point. It travels upward as a capillary wave and reaches the top of the droplet. Until this time the upper portion of the droplet does not move. In Fig. 3, $\tau = 1.53$ to $\tau = 2.18$ corresponds to the fast inertial spreading where the height of the droplet rapidly decreases. Also, it spreads rapidly over the porous surface. The simultaneous capillary penetration and viscous spreading is clearly visible at $\tau = 2.36$ to $\tau = 6.04$, where the rate of change of droplet height is low. Both the phenomena are comparatively very slow where capillary force is balanced by the viscous shear stress at the solid surfaces. In the next section, all these phenomena are quantitatively analyzed.

Droplet height (H)

The normalized droplet height (H/D) from the surface of the porous block with time (τ) is shown in Fig. 4 for varying contact angle (Θ) when $\varepsilon = 0.5$. For $\Theta = 30°$ and $\Theta = 45°$, three different zones, capillary wave propagation, fast inertial spreading; and then simultaneous viscous spreading and capillary penetration, can easily be observed. When $\Theta = 90°$, inertial spreading is rather small and the droplet interface oscillates at the end of the inertial spreading before it reaches the equilibrium condition. When the solid surfaces are made hydrophobic ($\Theta = 135°$), the height does not change much with time. At a first glance, it seems that there is no spreading. However, from the plot of spreading diameter (S) with time, the spreading can still be identified. This will be discussed in the next section. Fig. 5 shows the effect of porosity on transient variation of the droplet height when $\Theta = 45°$. Simulation results for the flat plate ($\varepsilon = 0$) are also shown. The effect of porosity on the transient variation of the droplet height is comparatively small. It is interesting to observe that with an increase in porosity, the rate of change of height ($\delta H/\delta\tau$) decreases. This phenomenon is also observed

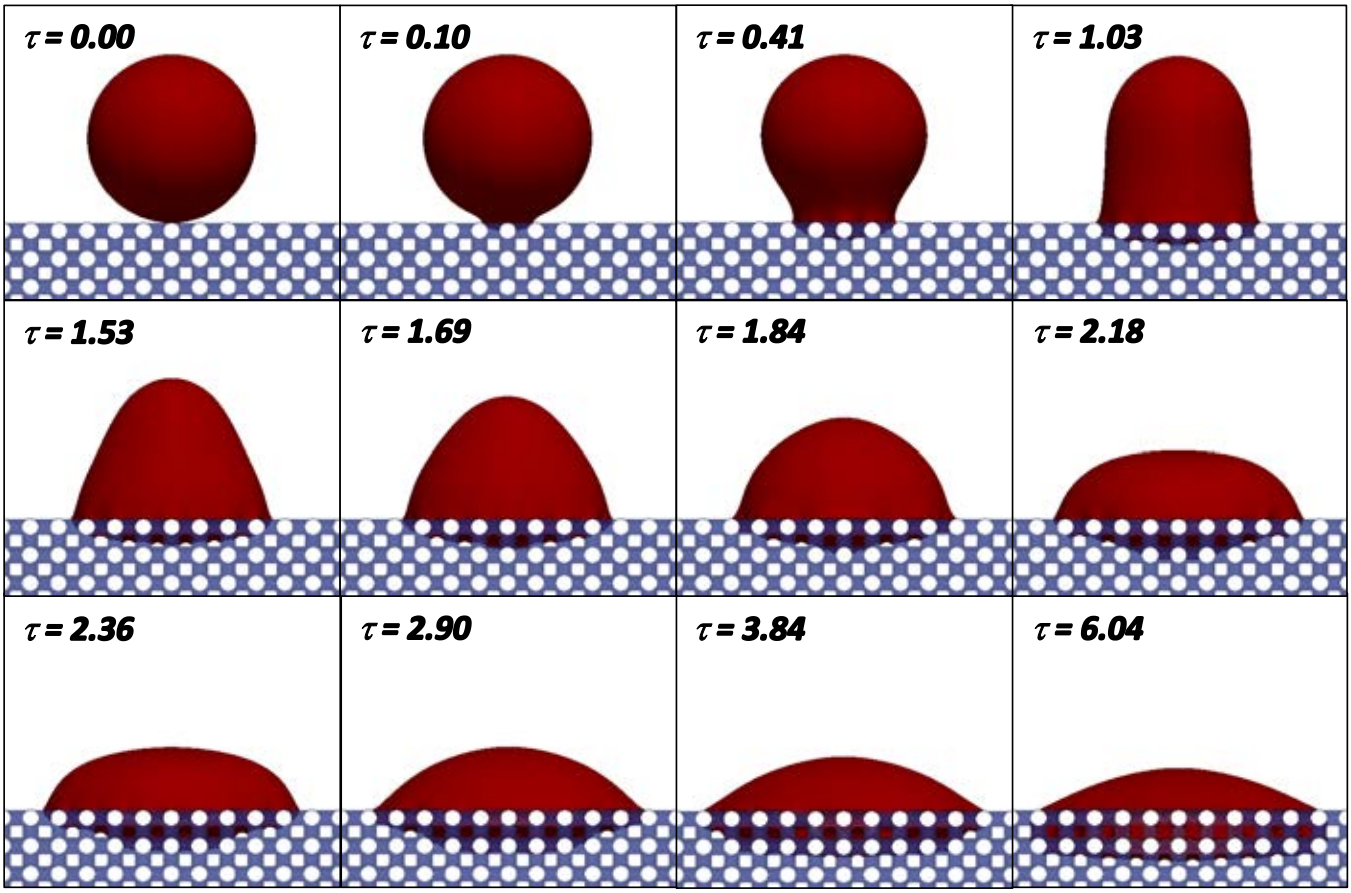

Figure 3: Droplet shape evolution during spreading and capillary penetration on a porous block of porosity $\varepsilon = 0.5$ and equilibrium contact angle $\Theta = 30^{\circ}$. τ is the non-dimensional time.

by Frank and Perre (2012) through LBM simulation. At a particular time, the total height of the droplet depends on both the inertial spreading and capillary penetration. When the porosity increases, the inertial spreading slows down while the capillary penetration increases. The time-scale for inertial spreading is high compared to the capillary penetration. Hence, the relative contribution of the inertial spreading is higher and mainly governs the height of the droplet. With decrease in the porosity, the inertial spreading increases and as a result the total height decreases faster.

Equivalent spreading diameter (S)

Unlike the droplet spreading over a flat plate, the imprint of the contact line on the surface of the porous block is not always circular. Based on the spread area, just above the porous block, we have calculated an equivalent spreading diameter (S) at each time-step. The variation of the normalized spreading diameter (S/D) with non-dimensional time (τ) is shown in Fig. 6 for varying Θ and in Fig. 7 for varying ε. Here too, it is very clearly visible that, for all the cases the inertial fast spreading lasts up to approximately $\tau \approx 2$. Similar to spreading over a flat surface, power-law variation of spreading, i.e. $S \sim C\tau^n$ is still valid for all the cases. From Fig. 6, we can observe that the spreading is faster when the contact angle is low and it is slower for the hydrophobic case. Fig. 7 clearly shows that spreading is fastest for the flat plate, slowed down with increasing

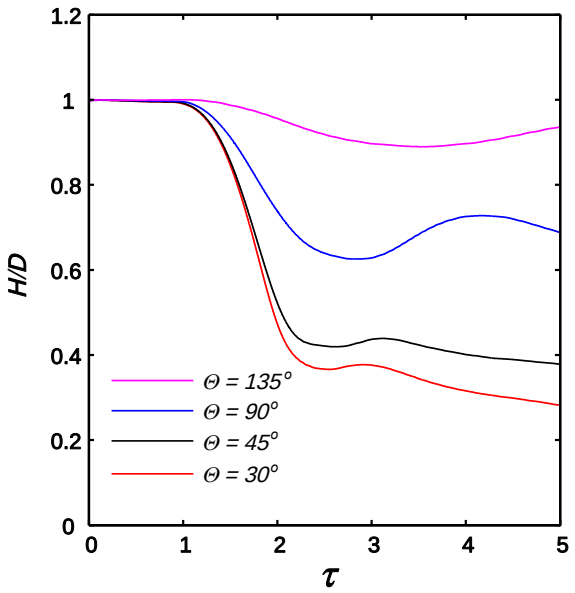

Figure 4: Droplet height (H/D) evolution for $\varepsilon = 0.5$: effect of Θ.

porosity. After the inertial spreading, S decreases slowly with time for higher porosity cases, due to capillary penetration of the liquid.

To study quantitatively, the effect of ε and Θ on spreading dynamics (S), both the exponent (n) and pre-factor (S) of the

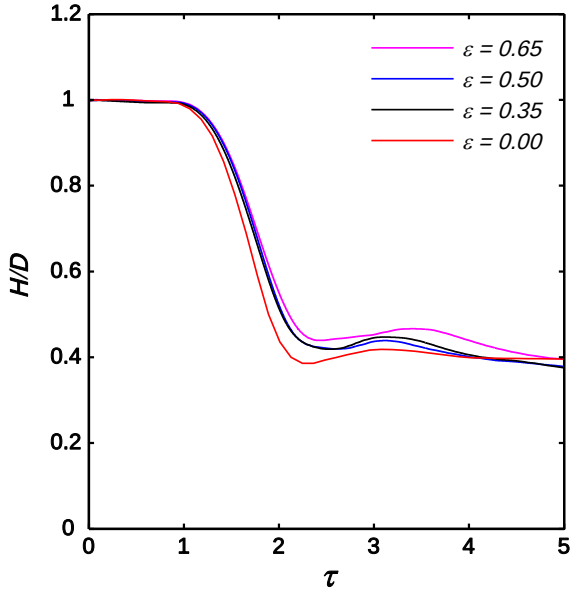

Figure 5: Droplet height (H/D) evolution for $\Theta = 45^{\circ}$: effect of ε.

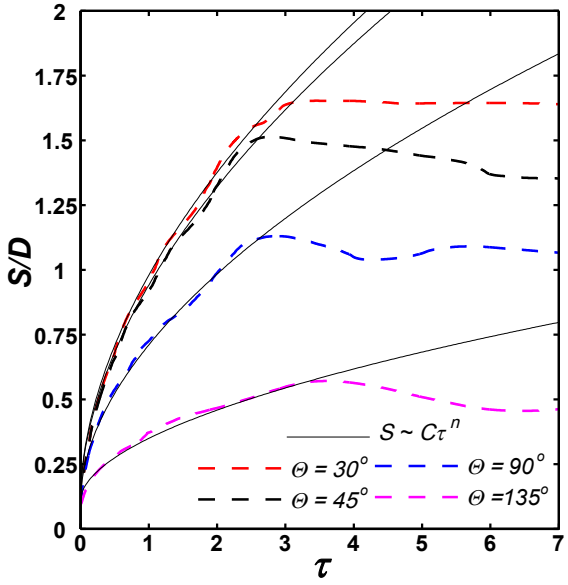

Figure 6: Evolution of equivalent spreading diameter (S/D) for ε = 0.5: effect of Θ.

$S/D = C\tau^n$ fit have been evaluated for all the cases. Fig. 8 shows the variation of n and S with ε and Θ. For spreading over a flat plate, for all the contact angle, Legendre (Legendre and Maglio, 2013) observed that n varies from 0.5 to 0.66 for $La = 72000$ to $La = 7$. In the present case, for $La = 45$, we found $n = 0.62$ for the case of flat plate. In our simulation it is observed that n is almost constant with Θ, however, decreases linearly with porosity. On the other hand, the pre-factor C decreases drastically with Θ, which indicated slower spreading for hydrophobic surfaces. The pre-factor C also decreases with increase in porosity, however, the variation is comparatively less.

Liquid penetration (V)

Finally, we have studied the amount of liquid penetration inside the porous block with time. The volume of penetrated liquid (V) normalized by the total volume of the droplet

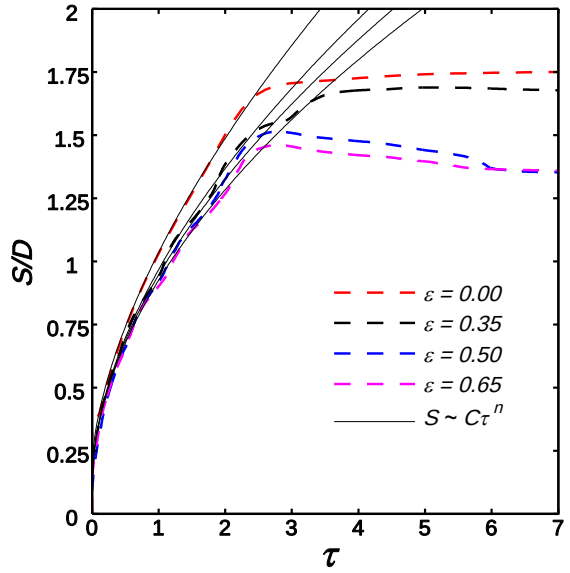

Figure 7: Evolution of equivalent spreading diameter (S/D) for Θ = 45°: effect of ε.

(V_0) is plotted against time in Fig. 9 for different Θ. For $\Theta = 30^{\circ}$ and $\Theta = 60^{\circ}$ the penetration is faster, the equilibrium condition is only reached when the full droplet drained into the porous block. For the rest of the cases, only a single layer of the porous block get wet by the liquid. An equilibrium condition is achieved when the contact force at the triple lines of the upper surface of the porous medium is balanced by the contact force inside the porous block.

Fig. 10 shows the effect of porosity on capillary penetration. For $\Theta = 60^{\circ}$, the equilibrium condition is achieved after only a small amount of liquid penetration. However, for $\Theta = 30^{\circ}$, the liquid penetration is faster and a strong function of ε. In this stage, the capillary force is balanced by the viscous forces. The magnitude of viscous resistance can be estimated by the Kozeny–Carman equation, which shows a non-linear increase in viscous resistance with an increase in solid fraction $(1 - \varepsilon)$. For higher porosity, the lower viscous resistance increases the capillary imbibition.

CONCLUSIONS

For the first time, the very complex interaction between a droplet and a porous media has been studied by an accurate IBM-VOF method based finite volume code. The complex physical phenomena, like contact line motion, inertial spreading, and capillary imbibition have been successfully studied, analysed and qualitatively compared with literature results for a range of porosities and contact angles. It is found that the transient behaviour of spreading follows a power law with time, similar to the droplet interaction with a flat plate. For smaller contact angles and lower porosities, the spreading is fast, which forces a quick reduction in droplet height in a short time. Irrespective of porosity, the capillary imbibition stalls for contact angle 60° and above. However, this limiting value depends on the geometrical details of the porous structures. Viscous penetration is comparatively slow, and the rate of volumetric imbibition is a strong function of the porosity. For the present moderate or low Laplace number simulations, the motion of the droplet is smooth,

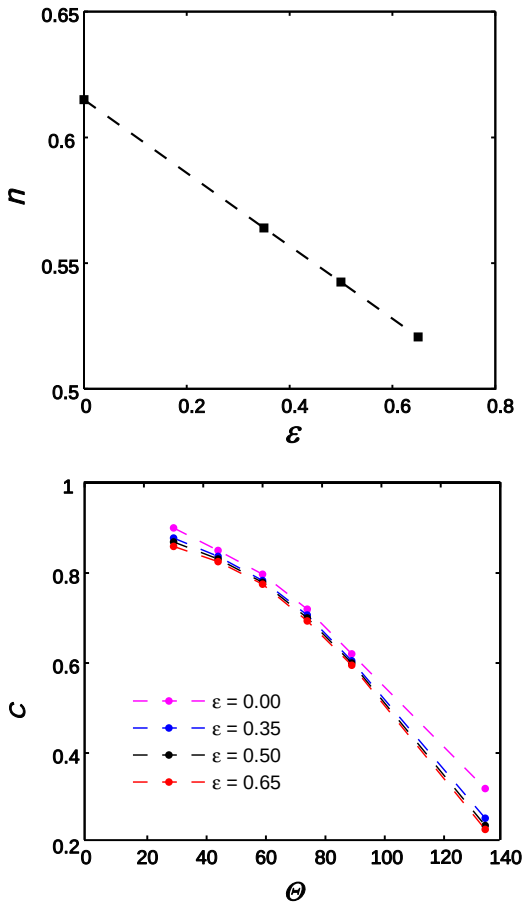

Figure 8: Exponent (n) and pre-factor (C) of power-law ($S/D = C\tau^n$) evolution of spreading diameter for different cases.

however, our code is also capable of simulating systems of very large Laplace number. In the next stage of our research, we intend to study the effect of Laplace number on droplet pinch-off and satellite droplet formation.

REFERENCES

BRACKBILL, J.U., KOTHE, D.B. and ZEMACH, C. (1992). "A continuum method for modeling surface tension". *Journal of computational physics*, **100(2)**, 335–354.

DAS, S., DEEN, N.G. and KUIPERS, J.A.M. (2016). "Immersed boundary method (ibm) based direct numerical simulation of open-cell solid foams: Hydrodynamics". *AIChE Journal*.

DEEN, N.G., KRIEBITZSCH, S.H., VAN DER HOEF, M.A. and KUIPERS, J.A.M. (2012). "Direct numerical simulation of flow and heat transfer in dense fluid–particle systems". *Chemical Engineering Science*, **81**, 329–344.

FRANK, X. and PERRE, P. (2012). "Droplet spreading on a porous surface: A lattice boltzmann study". *Physics of Fluids*, **24(4)**, 042101.

FRANK, X., PERRÉ, P. and LI, H.Z. (2015). "Lattice boltzmann investigation of droplet inertial spreading on various porous surfaces". *Physical Review E*, **91(5)**, 052405.

HYVÄLUOMA, J., RAISKINMÄKI, P., JÄSBERG, A., KOPONEN, A., KATAJA, M. and TIMONEN, J. (2006). "Simulation of liquid penetration in paper". *Physical Review E*, **73(3)**, 036705.

LEGENDRE, D. and MAGLIO, M. (2013). "Numerical simulation of spreading drops". *Colloids and Surfaces A: Physicochemical and Engineering Aspects*, **432**, 29–37.

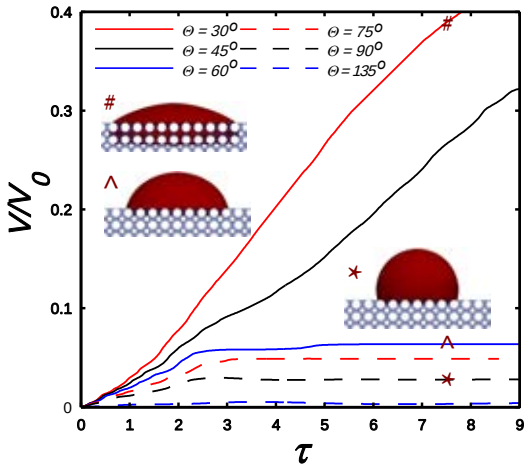

Figure 9: Volume of penetrated liquid (V/V_0) with time (τ) for ε = 0.35: effect of Θ.

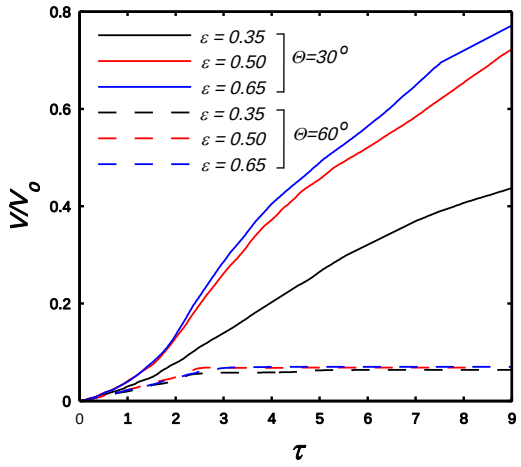

Figure 10: Volume of penetrated liquid (V/V_0) with time (τ) for $\Theta = 30^\circ$ and 60°: effect of ε.

MENG, S., YANG, R., WU, J.S. and ZHANG, H. (2014). "Simulation of droplet spreading on porous substrates using smoothed particle hydrodynamics". *International Journal of Heat and Mass Transfer*, **77**, 828–833.

PATEL, H., DAS, S., KUIPERS, J.A.M., PADDING, J.T. and PETERS, E.A.J.F. (2017). "A coupled volume of fluid and immersed boundary method for simulating 3d multiphase flows with contact line dynamics in complex geometries". *Chemical Engineering Science*.

TANNER, L. (1979). "The spreading of silicone oil drops on horizontal surfaces". *Journal of Physics D: Applied Physics*, **12(9)**, 1473.

VAN SINT ANNALAND, M., DEEN, N.G. and KUIPERS, J.A.M. (2005). "Numerical simulation of gas bubbles behaviour using a three-dimensional volume of fluid method". *Chemical Engineering Science*, **60(11)**, 2999–3011.

WINKELS, K.G., WEIJS, J.H., EDDI, A. and SNOEIJER, J.H. (2012). "Initial spreading of low-viscosity drops on partially wetting surfaces". *Physical Review E*, **85(5)**, 055301.

YANG, W. and XU, J. (2017). "Drop spreading and penetrating on micro/nano particle sintering porous with multiscale structure". *Colloids and Surfaces A: Physicochemical and Engineering Aspects*, **516**, 9–22.